LETTER

doi:10.1038/nature25144

Effector CD8 T cells dedifferentiate into long-lived memory cells

Ben Youngblood[1,2,3], J. Scott Hale[1,2], Haydn T. Kissick[4], Eunseon Ahn[1,2], Xiaojin Xu[1,2], Andreas Wieland[1,2], Koichi Araki[1,2], Erin E. West[1,2], Hazem E. Ghoneim[3], Yiping Fan[5], Pranay Dogra[3], Carl W. Davis[1,2], Bogumila T. Konieczny[1,2], Rustom Antia[6], Xiaodong Cheng[7]† & Rafi Ahmed[1,2]

Memory CD8 T cells that circulate in the blood and are present in lymphoid organs are an essential component of long-lived T cell immunity. These memory CD8 T cells remain poised to rapidly elaborate effector functions upon re-exposure to pathogens, but also have many properties in common with naive cells, including pluripotency and the ability to migrate to the lymph nodes and spleen. Thus, memory cells embody features of both naive and effector cells, fuelling a long-standing debate centred on whether memory T cells develop from effector cells or directly from naive cells[1–4]. Here we show that long-lived memory CD8 T cells are derived from a subset of effector T cells through a process of dedifferentiation. To assess the developmental origin of memory CD8 T cells, we investigated changes in DNA methylation programming at naive and effector cell-associated genes in virus-specific CD8 T cells during acute lymphocytic choriomeningitis virus infection in mice. Methylation profiling of terminal effector versus memory-precursor CD8 T cell subsets showed that, rather than retaining a naive epigenetic state, the subset of cells that gives rise to memory cells acquired *de novo* DNA methylation programs at naive-associated genes and became demethylated at the loci of classically defined effector molecules. Conditional deletion of the *de novo* methyltransferase Dnmt3a at an early stage of effector differentiation resulted in reduced methylation and faster re-expression of naive-associated genes, thereby accelerating the development of memory cells. Longitudinal phenotypic and epigenetic characterization of the memory-precursor effector subset of virus-specific CD8 T cells transferred into antigen-free mice revealed that differentiation to memory cells was coupled to erasure of *de novo* methylation programs and re-expression of naive-associated genes. Thus, epigenetic repression of naive-associated genes in effector CD8 T cells can be reversed in cells that develop into long-lived memory CD8 T cells while key effector genes remain demethylated, demonstrating that memory T cells arise from a subset of fate-permissive effector T cells.

We used the mouse model of acute lymphocytic choriomeningitis virus (LCMV) infection to examine the transcriptional and epigenetic changes that occur as naive CD8 T cells differentiate into effector and memory cells. It is well known that many effector genes are turned on when naive CD8 T cells are stimulated by antigen, but it is less well appreciated that several genes expressed by naive T cells are also turned off upon T cell activation[5,6]. Notably, several of these naive-associated genes that are downregulated in effector CD8 T cells are expressed by central memory cells. This on–off–on pattern of gene expression is shown for LCMV-specific effector and memory CD8 T cells in Fig. 1a. Among the genes that show this pattern are those encoding L-selectin (*Sell*, also known as *Cd62l*) (Fig. 1b) and CCR7, which are needed for homing to lymphoid organs, and BCL-2 and CD127, which are important for long-term survival of memory T cells[6,7]. To examine epigenetic changes associated with this on–off–on pattern, we analysed the DNA methylation profile of the *Sell* promoter. Previous studies have defined CpG sites in the *Sell* promoter region proximal to the binding sites for Klf2 and Ets1, two transcription factors known to regulate *Sell* expression[8,9] (Extended Data Fig. 1a). To determine whether the methylation status of these CpG sites has a direct effect on gene expression, we used a reporter construct to show that these CpG sites do regulate the expression of L-selectin (Extended Data Fig. 1b, c). Having established that methylation of these CpG sites decreases L-selectin expression *in vitro*, we next examined the methylation status of these sites in LCMV-specific naive, effector, and memory P14 CD8 T cells (T cell receptor (TCR) transgenic CD8 T cells specific to the LCMV gp33 epitope) during acute LCMV infection *in vivo* (Fig. 1c). Consistent with the high level of *Sell* transcription in naive CD8 T cells, the CpG sites proximal to the *Sell* promoter were completely unmethylated in naive cells, whereas the *Sell* promoter was significantly methylated in LCMV-specific effector CD8 T cells taken at either day 4 or day 8 of infection, which did not express L-selectin (Extended Data Fig. 1d). Notably, memory P14 cells showed minimal methylation at this promoter site and, consistent with this permissive epigenetic state, there was expression of *Sell* mRNA (Fig. 1c, Extended Data Fig. 1d, e). However, as more than 95% of effector CD8 T cells undergo apoptosis, it is possible that these surviving L-selectin-positive memory P14 cells may never have been methylated during the effector phase of the T cell response. The pool of effector CD8 T cells consists of two subsets; the majority (95%) are terminal effectors (TEs) that are destined to die, and the minority (5%), termed memory precursors (MPs), survive to give rise to the pool of long-lived memory T cells[5]. These two subsets can be distinguished on the basis of their expression of the cell surface markers Klrg1 and CD127[10–12]. We analysed the TE and MP effector subsets at day 8; notably, both subsets were equally methylated at the *Sell* promoter region and they also expressed low levels of *Sell* mRNA (Fig. 1d, Extended Data Fig. 1f, g). We next analysed memory cells at day 37 of infection and found that the L-selectin^{hi} population showed significant demethylation at the *Sell* promoter and expressed high levels of *Sell* mRNA (Fig. 1e, Extended Data Fig. 1f, h). Together, these results show that the MP effector CD8 T cell subset, which gives rise to memory cells, also becomes methylated at the *Sell* promoter during the acute phase of infection.

To obtain a more comprehensive assessment of methylation changes during naive-to-effector differentiation, we performed whole-genome bisulfite sequencing (WGBS) of antigen-specific MP and TE CD8 T cell subsets at days 4.5 and 8 (Extended Data Fig. 2a, b). Both effector subsets showed an increase in DNA methylation at about 1,000 regions

[1]Emory Vaccine Center, Emory University School of Medicine, Atlanta, Georgia 30322, USA. [2]Department of Microbiology and Immunology, Emory University School of Medicine, Atlanta, Georgia 30322, USA. [3]Department of Immunology, St. Jude Children's Research Hospital, Memphis, Tennessee 38105, USA. [4]Department of Urology, Emory University School of Medicine, Atlanta, Georgia 30322, USA. [5]Department of Computational Biology, St. Jude Children's Research Hospital, Memphis, Tennessee 38105, USA. [6]Department of Biology, Emory University, Atlanta, Georgia 30322, USA. [7]Department of Biochemistry, Emory University School of Medicine, Atlanta, Georgia 30322, USA. †Present address: Department of Molecular and Cellular Oncology, The University of Texas MD Anderson Cancer Center, Houston, Texas 77030, USA.

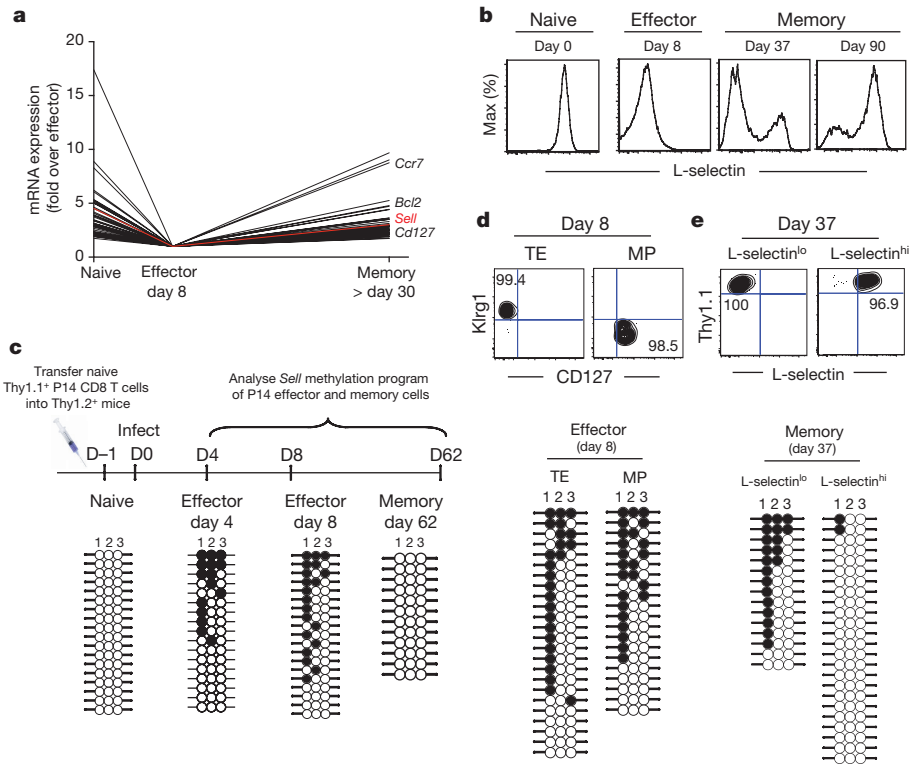

Figure 1 | Dynamic changes in DNA methylation during effector and memory CD8 T cell differentiation. a, Analysis of on–off–on gene expression from published microarray datasets for naive, LCMV-specific effector and LCMV-specific memory CD8 T cells[6]. **b**, Histogram analysis of L-selectin protein expression on naive, effector and memory P14 CD8 T cells following acute LCMV infection. **c**, Experimental setup and bisulfite sequencing DNA methylation analysis of the *Sell* promoter from P14 CD8 T cells purified (>95% purity) at the indicated stages of differentiation. Each horizontal line represents an individual sequenced clone. Filled circles, methylated cytosine; open circles, non-methylated cytosine. **d** Representative post-sort purity and DNA methylation analysis of *Sell* proximal promoter CpG sites in TE and MP P14 CD8 T cells FACS-purified 8 days after acute LCMV infection. **e**, Representative purification and DNA methylation analysis of effector memory (Tem) and central memory (Tcm) P14 CD8 T cells FACS-purified 37 days after acute LCMV infection. Statistical significance was determined from 3 or more biological replicates.

relative to naive cells, with marked enrichment of these methylation events near or within genes (Fig. 2a, Extended Data Fig. 3a). Most of these gain-of-methylation events occurred within the first 4 days of the effector response, and more than half of these differentially methylated regions (DMRs) were similarly acquired in both TE and MP effector cells. These DMRs included the previously defined sites in the *Sell* promoter as well as several other naive-associated genes, such as *Ccr7* and *Tcf7* (Fig. 2b). Thus, MP effector CD8 T cells, which are the precursors of memory cells, acquire repressive DNA methylation marks at many genes expressed by naive cells. Notably, the MP subset not only showed methylation of naive-associated genes, but also showed demethylation of several effector-associated genes, such as *Prf1*, granzyme genes and *Ifng* (Fig. 2c, d, Extended Data Fig. 4a–c). These results are consistent with a model in which MP cells transition through an effector phase during their differentiation into memory cells. Although there is a high degree of overlap between TE and MP subsets in effector-associated programming, there were also some notable differences in the level of demethylation (Extended Data Fig. 4d)—for example, a DMR in the *Prdm1* (also known as *Blimp1*) locus that remains methylated in the MP subset. This is consistent with prior reports showing that MP cells have lower *Prdm1* expression than TE cells and that deletion of *Prdm1* increases the number of effector cells with memory potential[13]. We also detected differential methylation of *Runx2* and *Runx3*, further suggesting that the fates of MP and TE cells are coupled to epigenetic programming of transcriptional regulators.

Having determined that epigenetic repression of naive-associated genes is a shared feature of both MP and TE CD8 T cells, we next investigated which enzyme(s) are involved in this DNA methylation. We hypothesized that the methylation would be *de novo*, because it was rapid and was retained even while the CD8 T cells were rapidly dividing (10–15 divisions) during the first week after infection[14]. Expression of the *de novo* methyltransferase Dnmt3a increases upon activation of CD8 T cells[15], so we tested whether Dnmt3a was required for methylation of the *Sell* promoter. To do this we used *Dnmt3a-Gzmb*–cre mice to conditionally knock out (cKO) *Dnmt3a* in virus-specific CD8 T cells following T cell activation *in vivo*[16,17] (Extended Data Fig. 5a). These *Dnmt3a* cKO mice were infected with LCMV; eight days after infection, virus-specific effector CD8 T cells were sorted using the LCMV gp33 tetramer (Extended Data Fig. 5b). PCR analysis of the *Dnmt3a* locus confirmed successful deletion of the enzyme (Extended Data Fig. 5c). We then assessed the methylation status of wild-type and cKO gp33 tetramer-positive effector CD8 T cells and found that in the absence of Dnmt3a there was no *de novo* methylation of the *Sell* promoter (Extended Data Fig. 5d). However, loss of Dnmt3a did not have any effect on maintenance methylation of a set of CpG sites distal to the *Sell* promoter (Extended Data Fig. 5e, f).

To more extensively profile loci targeted for *de novo* DNA methylation in effector cells, we performed WGBS with DNA from wild-type and *Dnmt3a* cKO antigen-specific effector CD8 T cells (Fig. 2e–g). Comparison of data from naive and wild-type effector cells revealed that the total pool of effector cells acquired about 2,000 newly methylated regions (Fig. 2e). Of these newly methylated regions, about 1,000 were verified as targets of Dnmt3a, as they were not acquired in *Dnmt3a* cKO effector cells (Fig. 2f). Many of these Dnmt3a targets were naive-associated genes such as *Sell*, *Ccr7* and *Tcf7* (Fig. 2g). In addition, several genes associated with regulating T cell lineage commitment and differentiation, including *Lef1* and *Il6st*, were also targets for effector-stage *de novo* methylation (Extended Data Fig. 6a). Unlike its

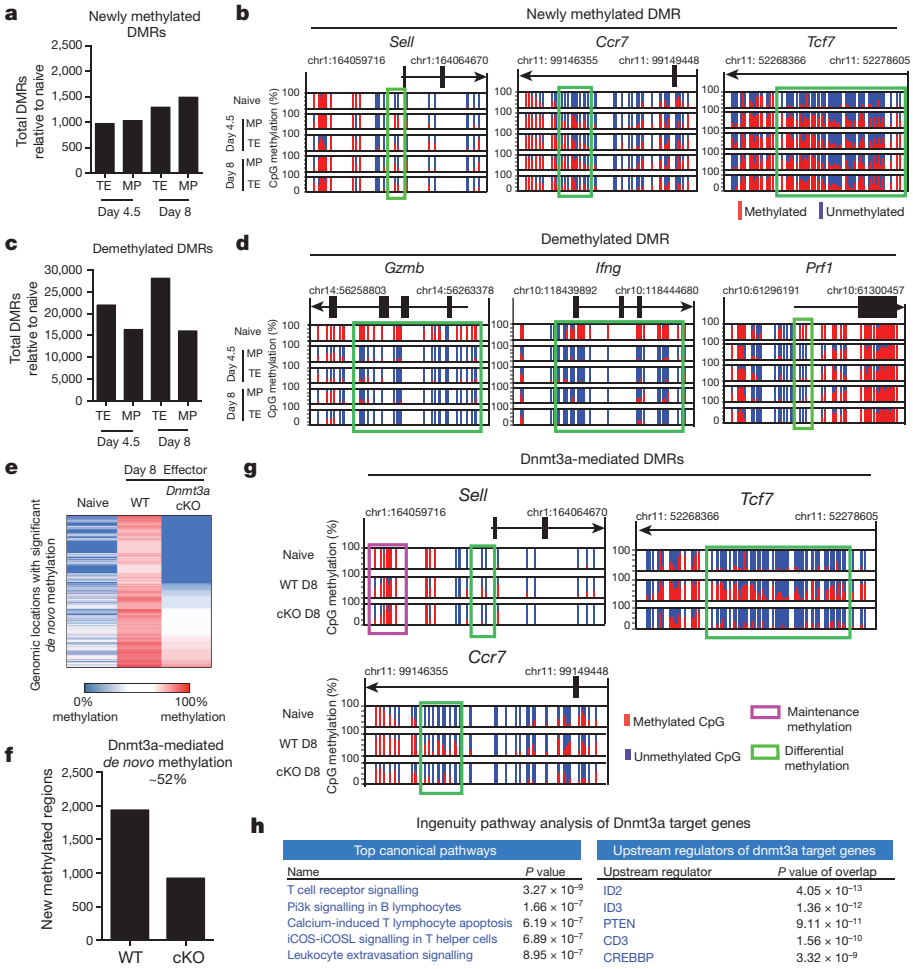

Figure 2 | MP CD8 T cells acquire genome-wide effector-associated DNA methylation programs. a, Summary of the number of newly methylated DMRs in TE and MP subsets relative to naive cells identified from WGBS analyses. **b**, Normalized CpG methylation in the *Ccr7*, *Tcf7*, and *Sell* loci from WGBS datasets. Each vertical line indicates a CpG site and the ratio of red to blue indicate the per cent of methylated versus unmethylated CpGs at these sites. **c**, Summary of the number of demethylation DMRs between the effector subsets and naive cells. **d**, Normalized methylation at CpG sites ini *Gzmb*, *Ifng* and *Prf1* loci from TE and MP WGBS datasets. **e**, Heat-map representation of the top 3,000 newly methylated regions (relative to naive CD8 T cell methylation) from WGBS analysis of tetramer^{+} wild-type and *Dnmt3a* cKO effector CD8 T cells. **f**, Summary of *de novo* methylated regions in wild-type and *Dnmt3a* cKO effector. **g**, Normalized Dnmt3a-mediated *de novo* methylation at CpG sites in the *Sell*, *Ccr7* and *Tcf7* loci. **h**, Top canonical pathways and upstream regulators from ingenuity pathway analysis of gene-associated Dnmt3a-mediated DMRs.

marked effect on *de novo* methylation, deletion of *Dnmt3a* did not have any effect on maintenance DNA methylation (Extended Data Fig. 6b). Given the selective nature of the Dnmt3a-targeted loci, we next assessed these genes for potential connections using ingenuity pathway analysis (IPA; Fig. 2h). Among the top canonical pathways identified by IPA were gene networks that were related to T cell receptor signalling and differentiation, further documenting the relationship between Dnmt3a-mediated programming and effector differentiation. Notably, our analysis revealed that loci targeted for *de novo* methylation were significantly associated with the transcription factors ID2 and ID3, two well-established regulators of effector and memory T cell differentiation[18,19] (Extended Data Fig. 6c). Collectively, these results demonstrate that downregulation of naive-associated genes is coupled to acquisition of Dnmt3a-mediated *de novo* DNA methylation programs during development of both MP and TE cells.

To determine how Dnmt3a-mediated *de novo* methylation regulates effector and memory T cell formation *in vivo*, we performed longitudinal analysis of the numbers and phenotypes of virus-specific CD8 T cells following LCMV infection of wild-type and *Dnmt3a* cKO mice. The magnitude of the virus-specific CD8 T cell response was similar in wild-type and *Dnmt3a* cKO mice; there were equivalent numbers of LCMV-specific CD8 T cells in multiple tissues at both effector and memory time points, and both groups of mice controlled the viral infection (Fig. 3a, Extended Data Fig. 7a–c). We confirmed that the memory cells in the *Dnmt3a* cKO mice were indeed deficient in Dnmt3a and did not represent an outgrowth of wild-type cells (Extended Data Fig. 7d). Thus, the magnitude of the virus-specific CD8 T cell response was not affected by Dnmt3a-mediated *de novo* methylation. Longitudinal analysis of phenotypic markers showed that L-selectin and CD127 were downregulated in both wild-type and *Dnmt3a* cKO effector cells eight days after infection (Fig. 3a, b, Extended Data Fig. 7e). Although the *Dnmt3a* cKO effector cells indeed lack the repressive DNA methylation programs, the transient downregulation of CD62L probably reflects the role of TCR signalling in promoting eviction of transcription factors from this promoter. However, following viral clearance, re-expression of L-selectin occurred significantly earlier in *Dnmt3a* cKO virus-specific CD8 T cells than in wild-type cells (Fig. 3b). *Dnmt3a* cKO CD8 T cells also showed enhanced conversion to a central memory phenotype compared to wild-type CD8 T cells (Fig. 3c). Similar to *Dnmt3a*-deficient cells in the peripheral blood, CD8 T cells in the spleen and lymph nodes of *Dnmt3a* cKO mice had significantly higher levels of *Sell* expression and contained more central memory cells when compared to those of wild-type mice (Fig. 3d, Extended Data Fig. 7f). Not only did *Dnmt3a* cKO mice

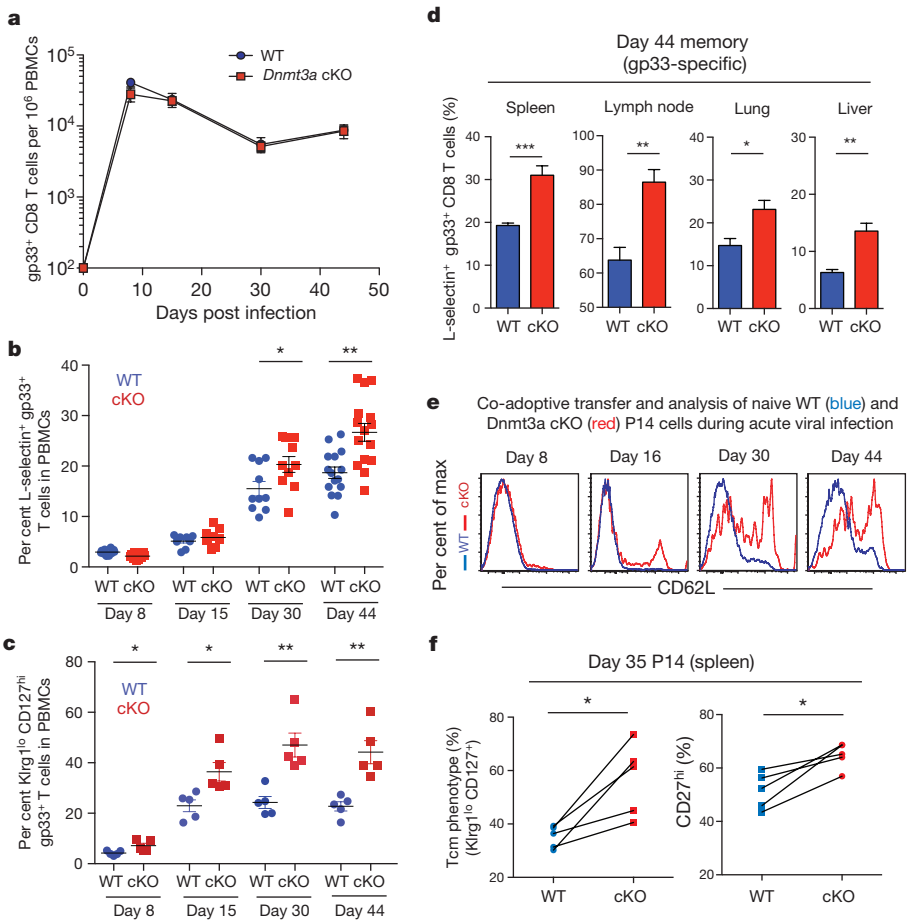

Figure 3 | Dnmt3a-mediated *de novo* DNA methylation regulates the kinetics of gene re-expression during the effector-to-memory CD8 T cell transition. a, Longitudinal measurement of numbers of wild-type and *Dnmt3a* cKO gp33-specific CD8 T cells in PBMCs during acute LCMV infection. **b**, **c**, Longitudinal analysis of central-memory (L-selectin^{hi}; **b**) and MP (Klrg1^{lo} L-selectin^{hi}; **c**) phenotypes of gp33-specific wild-type and *Dnmt3* cKO CD8 T cells in PBMCs ($n \geq 5$). **d**, Percentages of L-selectin-positive wild-type and *Dnmt3a* cKO gp33-specific memory CD8 T cells in the spleen and lymph node at 44 days after infection. **e**, Representative histogram analysis of L-selectin expression on wild-type (blue line) and *Dnmt3a* cKO (red line) P14 cells from the PBMCs of acutely infected chimaeric mice at 8, 16, 30, and 44 days after infection. **f**, Paired analysis of Klrg1^{lo} L-selectin^{hi} and L-selectin^{hi} phenotypes of wild-type and *Dnmt3a* cKO P14 splenocytes at 35 days post infection from co-transfer experiments ($n = 5$).

have significantly more L-selectin-positive memory CD8 T cells in lymphoid tissues than wild-type mice, but they also had a greater number of L-selectin-positive memory CD8 T cells in nonlymphoid tissues (lung and liver; Fig. 3d). Enhanced expression of L-selectin was also observed in LCMV-specific CD8 T cells that recognized the gp276 and np396 epitopes of the virus (Extended Data Fig. 7g).

We next investigated whether the faster re-expression of naive-associated genes in the *Dnmt3a* cKO cells compared to wild-type cells was due to a cell-intrinsic mechanism. *Dnmt3a* cKO mice were crossed with P14 transgenic mice to generate *Dnmt3a* cKO CD8 T cells with a TCR specific to the LCMV gp33 epitope. These *Dnmt3a* cKO naive P14 cells, along with congenically distinct wild-type naive P14 cells, were co-transferred into wild-type mice that were then acutely infected with LCMV (Fig. 3e). *Dnmt3a* cKO P14 cells showed similar downregulated *Sell* expression to wild-type P14 cells at 8 days after infection, but they re-expressed *Sell* much faster than did wild-type P14 cells (Fig. 3e). In addition, *Dnmt3a* cKO P14 cells exhibited an increased rate of conversion to central memory cells (CD127^{+} L-selectin^{+} CD27^{+} Klrg1^{lo}) compared to wild-type P14 cells (Fig. 3f). Thus, Dnmt3a intrinsically regulates the execution of the memory CD8 T cell program.

As *Dnmt3a* cKO cells showed faster conversion than wild-type cells to memory cells, we investigated the extent to which *Dnmt3a* cKO CD8 T cells underwent effector differentiation. We first assessed our whole-genome methylation analysis of day 8 cKO antigen-specific CD8 T cells for DNA demethylation events at effector-associated loci, including *Ifng*, *Prf1*, and *Gzmk*. Similar to the level of demethylation we observed in wild-type MP and TE cells, these loci were fully demethylated in the day 8 *Dnmt3a* cKO CD8 T cells, demonstrating that they had acquired effector-associated epigenetic programs (Extended Data Fig. 8a, b). The day 8 *Dnmt3a* cKO virus-specific CD8 T cells also expressed wild-type levels of Tbet (also known as Tbx21) and Ki67, providing further evidence that the *Dnmt3a* cKO cells had mounted an effector response (Extended Data Fig. 8c). Furthermore, the *Dnmt3a* cKO effector and memory cells were able to rapidly express effector cytokines upon *ex vivo* peptide stimulation (Extended Data Fig. 8d). These results explain the viral clearance data shown in Extended Data Fig. 7b, where we observed similar viral control in wild-type and *Dnmt3a* cKO mice.

Our results so far document that MP CD8 T cells not only demethylate effector-associated genes, but also methylate naive-associated genes. So a key question is whether virus-specific MP CD8 T cells that had downregulated naive-associated genes such as *Sell* re-express these genes and undergo associated epigenetic changes. To address this question, we isolated purified populations of L-selectin-negative day 8 P14 TE and MP cells, labelled them with carboxyfluorescein succinimidyl ester (CFSE) and adoptively transferred these cells into congenically distinct naive B6 mice (Fig. 4a). We then longitudinally tracked cell division, L-selectin expression, and promoter methylation of the transferred TE and MP populations. We took special care to avoid

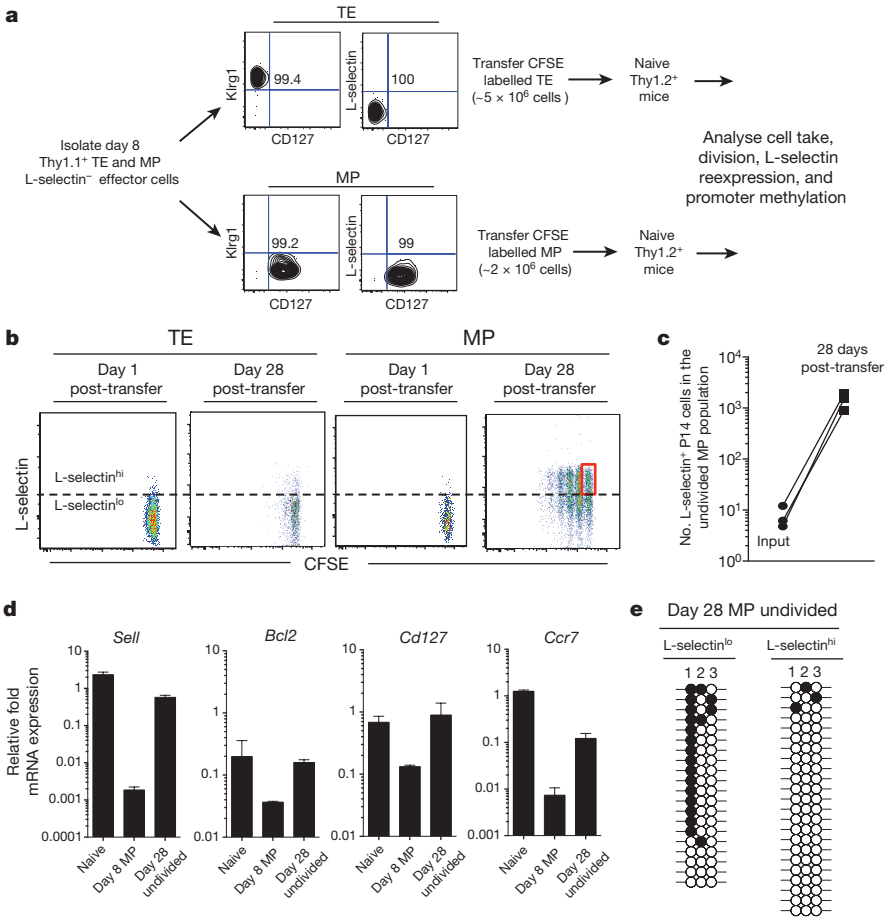

Figure 4 | Effector CD8 T cells erase Dnmt3a-mediated DNA methylation programs during their development into memory CD8 T cells. a, Experimental setup for obtaining CFSE-labelled TE and MP CD8 T cells at days 1 and 28 after transfer into naive mice. **b**, Representative FACS analysis of CFSE label and L-selectin expression of transferred TE and MP populations. **c**, Absolute numbers of transferred MP cells that were undivided and L-selectin-positive detected in the spleen on day 1 (input) and 28 days after transfer. **d**, Real-time PCR analysis of *Sell*, *Bcl2*, *CD127* and *Ccr7* from the indicated cell populations. **e**, Bisulfite sequencing DNA methylation analysis of the *Sell* promoter from the undivided L-selectin^{hi} versus L-selectin^{lo} memory populations.

transferring any L-selectin-positive cells by sorting only L-selectin-negative TE and MP P14 CD8 T cells (Fig. 4a). The take of the adoptively transferred TE and MP populations was determined by killing a group of recipient mice one day after cell transfer and quantifying the number of P14 cells in several lymphoid and non-lymphoid tissues. The CFSE-labelled transferred cells were present in all tissues analysed, and all of these cells were L-selectin-negative. No L-selectin-positive P14 cells were detected in any of the tissues examined (Extended Data Fig. 9a, b). Thus, on day 1 we began with a pure population of L-selectin-negative P14 TE and MP cells. Longitudinal tracking showed that 28 days after transfer the TE cell population mostly remained L-selectin-negative and did not divide (Fig. 4b). By contrast, many of the transferred MP cells now expressed L-selectin and were undergoing homeostatic proliferation (Fig. 4b, Extended Data Fig. 9c).

The most important finding from the above experiment was that even the undivided MP cells expressed L-selectin (Fig. 4b, red box), and there were more than 1,000 L-selectin-positive undivided P14 cells in the spleens of individual mice (Fig. 4c). As there were no detectable (fewer than 10) L-selectin-positive P14 cells at day 1 and we now had more than 1,000 L-selectin-positive P14 cells that had not undergone any division (that is, their presence could not be accounted for by any cell proliferation), the only possible explanation for the existence of these cells would be re-expression of L-selectin by previously L-selectin-negative MP effector cells. However, L-selectin protein can be cleaved from the surface of T cells, so we wanted to be sure that the increase in L-selectin was indeed due to an increase in *Sell* transcription and not simply due to lack of proteolytic cleavage of L-selectin. To this end, we sorted the undivided day 28 antigen-specific CD8 T cells and quantified mRNA expression levels compared to the input population of virus-specific MP cells. As shown in Fig. 4d, there was a 500-fold increase in the level of *Sell* mRNA in the undivided day 28 population compared to the input cells. In addition, these undivided day 28 cells had also upregulated several other naive-associated genes (*Bcl2*, *Ccr7*, *Il7r* (also known as *Cd127*)) that had been downregulated in the input population (Fig. 4d). Thus, these results provide unequivocal evidence that antigen-specific day 8 MP CD8 T cells can re-express naive-associated genes that have been downregulated during the effector phase.

We next sought to determine whether re-expression of L-selectin in the undivided CFSE^{+} memory CD8 T cells was coupled to demethylation of the promoter. Genomic DNA was isolated from sorted undivided L-selectin-positive and L-selectin-negative day 28 virus-specific memory CD8 T cells (Extended Data Fig. 9d) and the *Sell* promoter methylation status was analysed. Notably, the undivided L-selectin-positive memory population acquired a demethylated *Sell* promoter, whereas the L-selectin-negative memory cells retained a level of promoter methylation equivalent to that of input effector cells (Fig. 4e). These data demonstrate that erasure of the previously acquired *de novo* DNA methylation program at the *Sell* promoter in CD8 T cells occurs concordantly with re-expression of L-selectin during the effector-to-memory transition. Together, these results support the idea that memory CD8 T cells are generated through a process of cellular

dedifferentiation that allows the re-expression of naive-associated genes.

As shown in Fig. 2 and Extended Data Fig. 4, MP CD8 T cells showed demethylation of many canonical effector genes, including *Prf1* and *Gzmb*. To determine the methylation status of these effector genes in memory cells, virus-specific effector and memory CD8 T cells were isolated from mice 8 and 40 days after LCMV infection and the methylation status of the *Gzmb* and *Prf1* DMRs was measured. Notably, both *Gzmb* and *Prf1* loci remained demethylated in memory CD8 T cells (Extended Data Fig. 10a, b) even though these memory cells did not express high levels of perforin or granzyme b. Thus, these demethylation marks at effector genes are retained in memory cells.

The formation of memory CD8 T cells has been a topic of much interest, and debate over contrasting models of memory differentiation. One model describes effector and memory differentiation as distinct lineages arising from asymmetric cell division of the original naive T cell, allowing memory T cells to retain gene expression programs from the naive parental cell[2,20,21]. A contrasting model describes memory T cell differentiation as a process whereby memory CD8 T cells arise from a subset of effector cells (MP cells) that have the ability to re-acquire key naive-like properties and still retain the ability to rapidly elaborate effector functions[2,22]. Our results reveal that repression of the naive transcriptional program in MP effector cells is coupled to *de novo* DNA methylation of genes, which can then be erased as these cells re-acquire specific aspects of the naive-like gene expression program. Furthermore, we show that effector stage conditional deletion of the *de novo* DNA methyltransferase Dnmt3a results in enhanced kinetics for development of memory cells. A recent study examining the role of Dnmt3a during T cell differentiation also reports that *de novo* DNA methylation programs regulate the development of memory CD8 T cells. However, the authors of this study conclude that TE cells acquire *de novo* programs at critical loci, including *Tcf7*, but the MP cells lack these *de novo* programs[23]. By contrast, we show here that MP cells also acquire Dnmt3a-mediated methylation programs but have the capacity to erase their newly acquired methylation programs and re-express naive genes as they develop into memory CD8 T cells. Our findings do not argue against a model of memory T cell differentiation in which MP and TE cells undergo fate specification early in their development[24]. However, our results provide evidence that the MP subset of effector CD8 T cells can dedifferentiate into memory T cells. In an accompanying manuscript[25], we show that human virus-specific CD8 T cells also follow a similar program of memory differentiation and that both mouse and human memory CD8 T cells retain an epigenetic signature of their past effector history.

Online Content Methods, along with any additional Extended Data display items and Source Data, are available in the online version of the paper; references unique to these sections appear only in the online paper.

Received 3 November 2015; accepted 17 November 2017.
Published online 13 December 2017.

1. Obar, J. J. & Lefrançois, L. Memory CD8$^+$ T cell differentiation. *Ann. NY Acad. Sci.* **1183,** 251–266 (2010).
2. Ahmed, R., Bevan, M. J., Reiner, S. L. & Fearon, D. T. The precursors of memory: models and controversies. *Nat. Rev. Immunol.* **9,** 662–668 (2009).
3. Buchholz, V. R. *et al.* Disparate individual fates compose robust CD8$^+$ T cell immunity. *Science* **340,** 630–635 (2013).
4. Gerlach, C. *et al.* Heterogeneous differentiation patterns of individual CD8$^+$ T cells. *Science* **340,** 635–639 (2013).
5. Kaech, S. M., Hemby, S., Kersh, E. & Ahmed, R. Molecular and functional profiling of memory CD8 T cell differentiation. *Cell* **111,** 837–851 (2002).
6. Wherry, E. J. *et al.* Molecular signature of CD8$^+$ T cell exhaustion during chronic viral infection. *Immunity* **27,** 670–684 (2007).
7. Wirth, T. C. *et al.* Repetitive antigen stimulation induces stepwise transcriptome diversification but preserves a core signature of memory CD8$^+$ T cell differentiation. *Immunity* **33,** 128–140 (2010).
8. Dang, X., Raffler, N. A. & Ley, K. Transcriptional regulation of mouse L-selectin. *Biochim. Biophys. Acta* **1789,** 146–152 (2009).
9. Carlson, C. M. *et al.* Kruppel-like factor 2 regulates thymocyte and T-cell migration. *Nature* **442,** 299–302 (2006).
10. Kaech, S. M. *et al.* Selective expression of the interleukin 7 receptor identifies effector CD8 T cells that give rise to long-lived memory cells. *Nat. Immunol.* **4,** 1191–1198 (2003).
11. Sarkar, S. *et al.* Functional and genomic profiling of effector CD8 T cell subsets with distinct memory fates. *J. Exp. Med.* **205,** 625–640 (2008).
12. Joshi, N. S. *et al.* Inflammation directs memory precursor and short-lived effector CD8$^+$ T cell fates via the graded expression of T-bet transcription factor. *Immunity* **27,** 281–295 (2007).
13. Rutishauser, R. L. *et al.* Transcriptional repressor Blimp-1 promotes CD8$^+$ T cell terminal differentiation and represses the acquisition of central memory T cell properties. *Immunity* **31,** 296–308 (2009).
14. Murali-Krishna, K. *et al.* Counting antigen-specific CD8 T cells: a reevaluation of bystander activation during viral infection. *Immunity* **8,** 177–187 (1998).
15. Youngblood, B. *et al.* Chronic virus infection enforces demethylation of the locus that encodes PD-1 in antigen-specific CD8$^+$ T cells. *Immunity* **35,** 400–412 (2011).
16. Okano, M., Bell, D. W., Haber, D. A. & Li, E. DNA methyltransferases Dnmt3a and Dnmt3b are essential for *de novo* methylation and mammalian development. *Cell* **99,** 247–257 (1999).
17. Jacob, J. & Baltimore, D. Modelling T-cell memory by genetic marking of memory T cells *in vivo*. *Nature* **399,** 593–597 (1999).
18. Cannarile, M. A. *et al.* Transcriptional regulator Id2 mediates CD8$^+$ T cell immunity. *Nat. Immunol.* **7,** 1317–1325 (2006).
19. Yang, C. Y. *et al.* The transcriptional regulators Id2 and Id3 control the formation of distinct memory CD8$^+$ T cell subsets. *Nat. Immunol.* **12,** 1221–1229 (2011).
20. Chang, J. T. *et al.* Asymmetric T lymphocyte division in the initiation of adaptive immune responses. *Science* **315,** 1687–1691 (2007).
21. Arsenio, J. *et al.* Early specification of CD8$^+$ T lymphocyte fates during adaptive immunity revealed by single-cell gene-expression analyses. *Nat. Immunol.* **15,** 365–372 (2014).
22. Youngblood, B., Hale, J. S. & Ahmed, R. T-cell memory differentiation: insights from transcriptional signatures and epigenetics. *Immunology* **139,** 277–284 (2013).
23. Ladle, B. L. K., *et al. De novo* DNA methylation by DNA methyltransferase 3a controls early effector CD8$^+$ T -cell fate decisions following activation. *Proc. Natl Acad. Sci. USA* **113,** 10631–10636 (2016).
24. Chang, J. T. *et al.* Asymmetric proteasome segregation as a mechanism for unequal partitioning of the transcription factor T-bet during T lymphocyte division. *Immunity* **34,** 492–504 (2011).
25. Akondy R. S. *et al.* Origin and differentiation of human memory CD8 T cells after vaccination. *Nature* http://doi.org/10.1038/nature24633 (2017).

Supplementary Information is available in the online version of the paper.

Acknowledgements We thank R. Karaffa and S. Durham at the Emory University School of Medicine Flow Cytometry Core Facility and R. Cross and G. Lennon in the St Jude Flow Cytometry Core Facility for FACS sorting. Whole-genome sequencing was performed by the St Jude Hartwell Sequencing facility. This work was supported by the National Institutes of Health (NIH) grant U19 AI117891 (to R.An.), R01AI030048 (to R.Ah.), U19AI057266 (to R.Ah.), R01AI114442(to B.Y.), and funds from American Lebanese Syrian Associated Charities (ALSAC) (to B.Y.).

Author Contributions B.Y. and J.S.H. designed experiments, collected, analysed data and interpreted results. H.T.K. analysed data and interpreted results. E.E.W., E.A., X.X. and A.W. collected data, analysed data and interpreted results. Y.F., K.A., X.C. and R.An. interpreted results. H.E.G., P.D., C.W.D. & B.T.K. collected data. R.Ah. designed experiments and supervised the study. All authors contributed to the preparation of the manuscript.

Author Information Reprints and permissions information is available at www.nature.com/reprints. The authors declare no competing financial interests. Readers are welcome to comment on the online version of the paper. Publisher's note: Springer Nature remains neutral with regard to jurisdictional claims in published maps and institutional affiliations. Correspondence and requests for materials should be addressed to R.Ah. (rahmed@emory.edu) or B.Y. (benjamin.youngblood@stjude.org).

METHODS

No statistical methods were used to predetermine sample size. The experiments were not randomized and the investigators were not blinded to allocation during experiments and outcome assessment.

Generation of antigen-specific T cells. Wild-type male or female C57BL/6 mice (Jackson Laboratory), aged 6–8 weeks, were acutely infected with the Armstrong strain of LCMV (2×10^5 plaque-forming units (p.f.u.), intraperitoneal injection (i.p.)). Effector and memory antigen-specific CD8 T cells were identified and purified by FACS using H-2D^b tetramers bound to LCMV peptide gp33-41 conjugated to a fluorophore, along with CD8, CD44, CD127, Klrg1 and L-selectin–fluorophore conjugated antibodies as previously described[11,14,26,27]. To generate LCMV-specific CD8 T cell chimaeras, transgenic P14 CD8 T cells with an engineered TCR that recognizes the epitope gp33-41 of LCMV were collected from naive P14 TCR transgenic mice and adoptively transferred intravenously into C57BL/6 mice (cell numbers per mouse are specified in the figure legends)[11,28–30]. Congenically marked LCMV-specific CD8 T cells were sorted using fluorescently labelled CD90.1 (Thy1.1) and CD8 antibodies as previously described[14]. Naive antigen-specific cells obtained from transgenic P14 mice[31] were used as an antigen-specific naive control. *Dnmt3a* cKO mice were generated by breeding previously characterized floxed *Dnmt3a* mice with mice that contain a granzyme B-driven recombinase transgene[17,32]. Genotyping and recombination of the *Dnmt3a* locus were performed using primers listed in Supplementary Table 1. All mouse experiments were approved by Emory University Institutional Animal Care and Use Committee (IACUC).

Bisulfite sequencing methylation analysis. DNA was isolated from FACS-purified antigen-specific CD8 T cells using the Qiagen DNeasy kit. Genomic DNA was bisulfite-treated using the Zymo Research EZ DNA methylation kit. Bisulfite-induced deamination of cytosine was used to determine the allelic frequency of cytosine methylation of the target genomic region[33]. The bisulfite-modified DNA was PCR amplified with locus specific primers (Supplementary Table 1). The PCR amplicon was cloned into the pGEM-T TA cloning vector (Promega) then transformed into XL10-Gold ultracompetent bacteria (Stratagene). Individual bacterial colonies were grown and the cloning vector was isolated and sequenced.

Genome-wide methylation analysis. Genomic DNA from FACS-purified wild-type naive P14, day 4.5 TE and MP effector P14, day 8 TE and MP effector P14, day 8 total tetramer$^+$ wild-type and *Dnmt3a* cKO effector, and day 35 tetramer$^+$ wild-type memory CD8 T cells was isolated using the Qiagen DNeasy kit. Genomic DNA was bisulfite-treated using the Zymo Research EZ DNA methylation kit. The bisulfite-modified DNA sequencing library was generated using the Epicentre kit per the manufacturer's instructions. Bisulfite-modified DNA libraries were sequenced using an Illumina Hiseq. Sequencing was performed to yield more than 5× average coverage across the genome. Sequencing data were aligned to the mm10 mouse genome using BSMAP2.74[34]. Differentially methylated regions (DMRs) were identified using Bioconductor package DSS[35]. We first performed statistical tests of differentially methylated loci (DML) using DMLtest function (smoothing = TRUE) in DSS; the results were then used to detect differentially methylated regions using CallDMR function in DSS, with a P threshold for calling DMR set at 0.01. The minimum length for a DMR was set to 50 bp with a minimum number of three CpG sites. Genomic location classification was defined on the basis of RefSeq annotation as follows: promoter from within −2 kb to 1 kb of transcriptional start site (TSS), TSS proximal enhancer from −10 kb to −2 kb of TSS, distal from transcriptional termination site (TTS) from 1 kb to 2 kb of TTS, introns and exons defined in RefSeq annotation, and any other genomic regions were defined as intergenic. The distance was defined according to the strand of the gene. Each DMR was assigned in the order listed above and each DMR was assigned to one category only. The ShuffleBed function in bedtools[36] was used to generate a set of random regions of the same number and size distribution as the original DMRs to assess enrichment of DMR distribution among relative genomic locations. Specifically, each DMR was repositioned on a random chromosome at a random position. The number of DMRs and the size of DMRs were preserved. The random set of regions was then annotated in the same way as the original DMRs. Differential methylation analysis of CpG methylation among the datasets was further assessed using a Bayesian hierarchical model to detect differences among methylation at three CpG sites[37].

Real-time PCR analysis of mRNA. Splenocytes were collected from mice at the described time points after infection with LCMV. Antigen-specific CD8 T cells were purified by FACS. RNA was extracted from cells using the Qiagen RNeasy kit per the manufacturer's instructions. Quantitative real-time PCR of *Sell* was performed using primers that have been previously described[38].

***In vivo* cellular proliferation.** Virus-specific CD8 T cells were FACS-purified and resuspended in PBS at a concentration of 2×10^7 per ml. One volume of 5 μM CFSE was mixed with one volume of cells for 7 min at room temperature. 100% fetal calf serum was added to the cell suspension at final volume of 20% to quench the labelling. Cells were washed with PBS once and then adoptively transferred into naive B6 mice.

***In vitro* promoter methylation and expression assay.** The pCpGfree-basic reporter construct was purchased from InVivogen and the *Sell* promoter was cloned into the MCS of the reporter construct. Proper orientation of the promoter was confirmed by sequencing. *In vitro* methylation of the plasmid was performed using MSsI purchased from New England Biolabs. The plasmid was incubated with the enzyme and cofactor for 2 h at 37 °C and then additional cofactor was spiked into the reaction before incubation for another 2 h. Methylation was confirmed using the established *Sell* bisulfite sequencing assay. Unmethylated and *in vitro* methylated plasmids (0.5 μg) were then transfected into EL4 cells (this cell line was purchased from ATCC but was not independently confirmed or tested for mycoplasma contamination) using Lipofectamine 2000 according to the manufacturer's instructions. Supernatant was isolated from the cell culture at various times and the Lucia activity was measured using Quantiluc reagent on a Veritas luminometer.

Statistical significance for all *in vivo* and *in vitro* studies, excluding the WGBS analyses, was determined on three or more biological replicate samples using Prism software. P values were determined using a two-tailed Student's t-test. $^*P < 0.05$; $^{**}P < 0.01$; $^{***}P < 0.001$.

Data availability. The data that support the findings of this study are available from the corresponding author upon request. Whole-genome bisulfite sequencing datasets can be obtained from the NCBI Gene Expression Omnibus (accession no. GSE107150).

26. Wherry, E. J., Blattman, J. N., Murali-Krishna, K., van der Most, R. & Ahmed, R. Viral persistence alters CD8 T-cell immunodominance and tissue distribution and results in distinct stages of functional impairment. *J. Virol.* **77,** 4911–4927 (2003).
27. Matloubian, M., Somasundaram, T., Kolhekar, S. R., Selvakumar, R. & Ahmed, R. Genetic basis of viral persistence: single amino acid change in the viral glycoprotein affects ability of lymphocytic choriomeningitis virus to persist in adult mice. *J. Exp. Med.* **172,** 1043–1048 (1990).
28. Blattman, J. N. *et al.* Estimating the precursor frequency of naive antigen-specific CD8 T cells. *J. Exp. Med.* **195,** 657–664 (2002).
29. Kersh, E. N. Impaired memory CD8 T cell development in the absence of methyl-CpG-binding domain protein 2. *J. Immunol.* **177,** 3821–3826 (2006).
30. Kersh, E. N. *et al.* Rapid demethylation of the IFN-γ gene occurs in memory but not naive CD8 T cells. *J. Immunol.* **176,** 4083–4093 (2006).
31. Pircher, H., Bürki, K., Lang, R., Hengartner, H. & Zinkernagel, R. M. Tolerance induction in double specific T-cell receptor transgenic mice varies with antigen. *Nature* **342,** 559–561 (1989).
32. Kaneda, M. *et al.* Essential role for *de novo* DNA methyltransferase Dnmt3a in paternal and maternal imprinting. *Nature* **429,** 900–903 (2004).
33. Trinh, B. N., Long, T. I. & Laird, P. W. DNA methylation analysis by MethyLight technology. *Methods* **25,** 456–462 (2001).
34. Xi, Y. & Li, W. BSMAP: whole genome bisulfite sequence MAPping program. *BMC Bioinformatics* **10,** 232 (2009).
35. Wu, H. *et al.* Detection of differentially methylated regions from whole-genome bisulfite sequencing data without replicates. *Nucleic Acids Res.* **43,** e141 (2015).
36. Quinlan, A. R. & Hall, I. M. BEDTools: a flexible suite of utilities for comparing genomic features. *Bioinformatics* **26,** 841–842 (2010).
37. Feng, H., Conneely, K. N. & Wu, H. A Bayesian hierarchical model to detect differentially methylated loci from single nucleotide resolution sequencing data. *Nucleic Acids Res.* **42,** e69 (2014).
38. Furukawa, Y. *et al.* Identification of novel isoforms of mouse L-selectin with different carboxyl-terminal tails. *J. Biol. Chem.* **283,** 12112–12119 (2008).

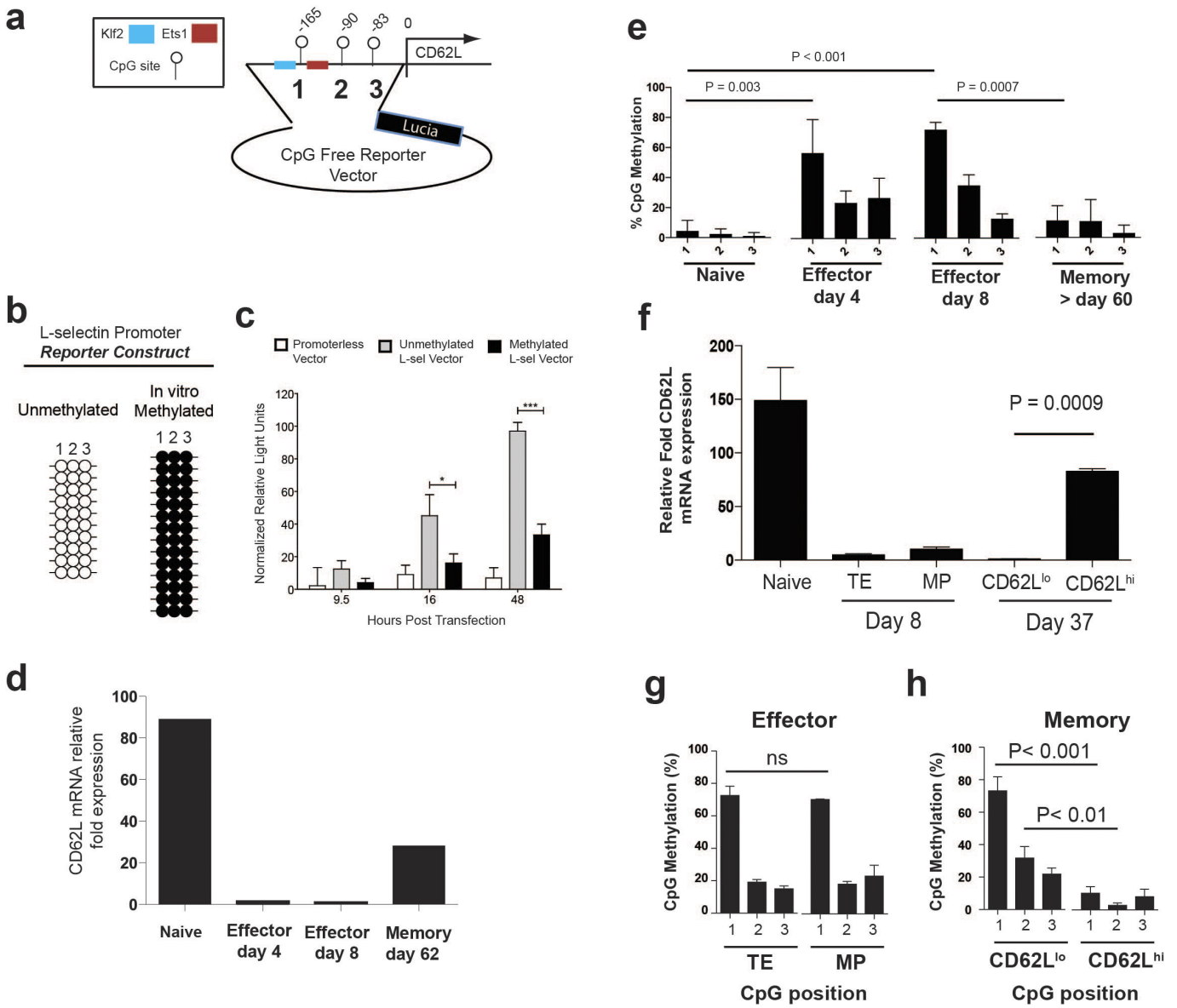

Extended Data Figure 1 | *Sell* gene expression changes during effector and memory CD8 T cell differentiation are coupled to epigenetic reprogramming of the *Sell* promoter. a, Cartoon of CpG positions within the *Sell* promoter region cloned into the CpG-free Lucia Promoter reporter construct. Putative transcription factor binding sites are indicated by coloured boxes. **b**, Representative methylation profiling of *in vitro* methylation efficiency of the reporter construct. **c**, Longitudinal measurement of relative light units from EL4 cells transfected with unmethylated and *in vitro* methylated reporter constructs. **d**, Real-time PCR analysis of *Sell* mRNA in virus-specific naive, effector, and memory P14 CD8 T cells. **e**, Summary of *Sell* proximal promoter methylation in naive, day 4 effector, day 8 effector and day 60+ memory P14 CD8 T cells. Each horizontal line represents an individual sequenced clone. Filled circles, methylated cytosine; open circles, non-methylated cytosine. **f**, Real-time PCR analysis of *Sell* mRNA expression from day 8 TE and MP P14 CD8 T cells, and day 37 L-selectin^{lo} and L-selectin^{hi} P14 CD8 T cells. Transcript data correspond to cell sorts used for DNA methylation measurements in Fig. 1f, h. **g**, **h**, Summary of *Sell* proximal promoter DNA methylation in TE and MP effector CD8 T cells and L-selectin^{lo} and L-selectin^{hi} memory CD8 T cells. Statistics were generated from three or more biological replicates.

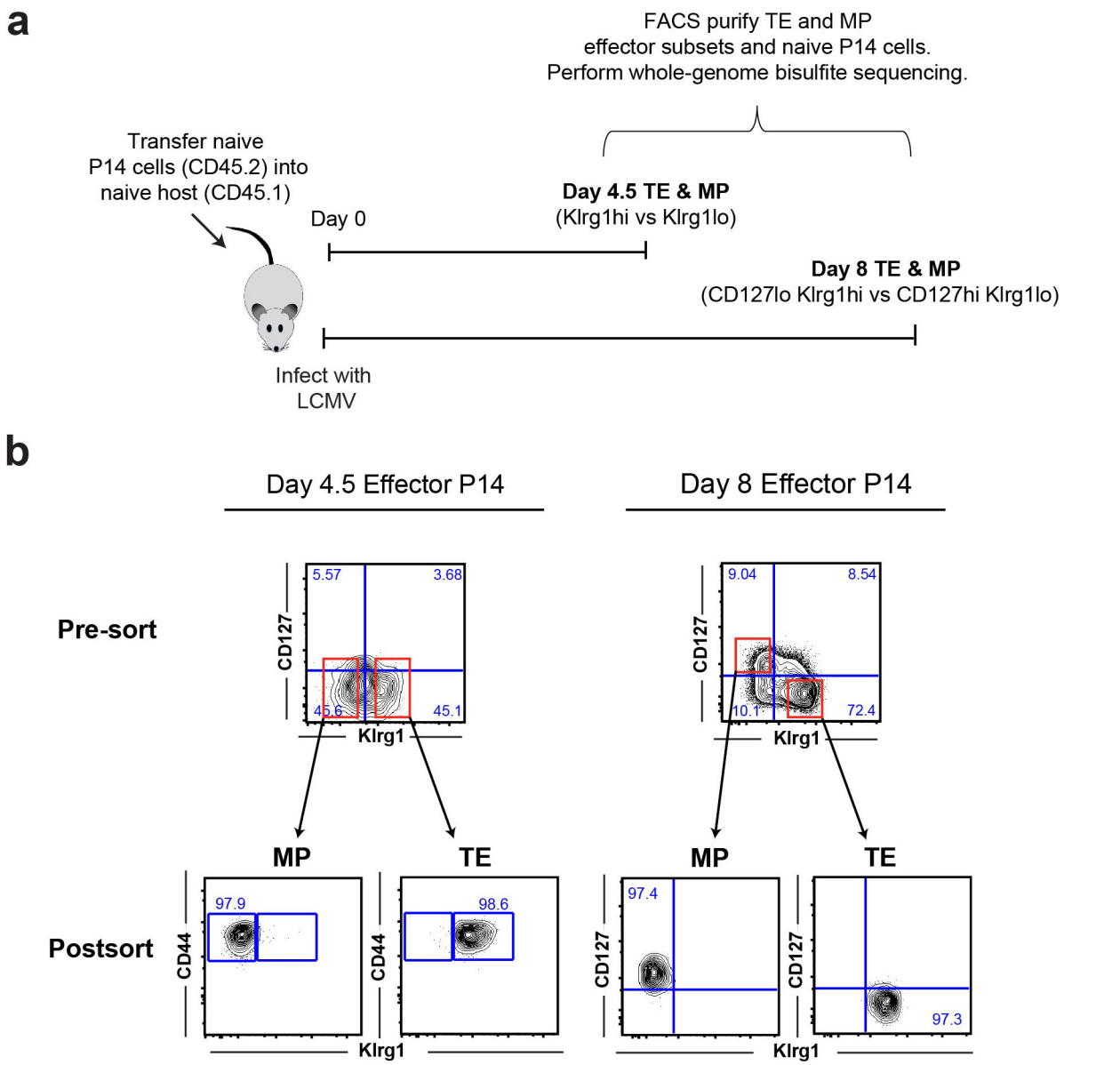

Extended Data Figure 2 | Isolation of MP and TE CD8 T cells for whole-genome methylation profiling. a, Experimental setup for isolating MP and TE LCMV-specific CD8 T cells on days 4.5 and 8. **b**, Representative post-sort purity and phenotypic analysis of day 4.5 and day 8 MP and TE P14 CD8 T cells isolated from acutely infected mice used for WGBS methylation profiling.

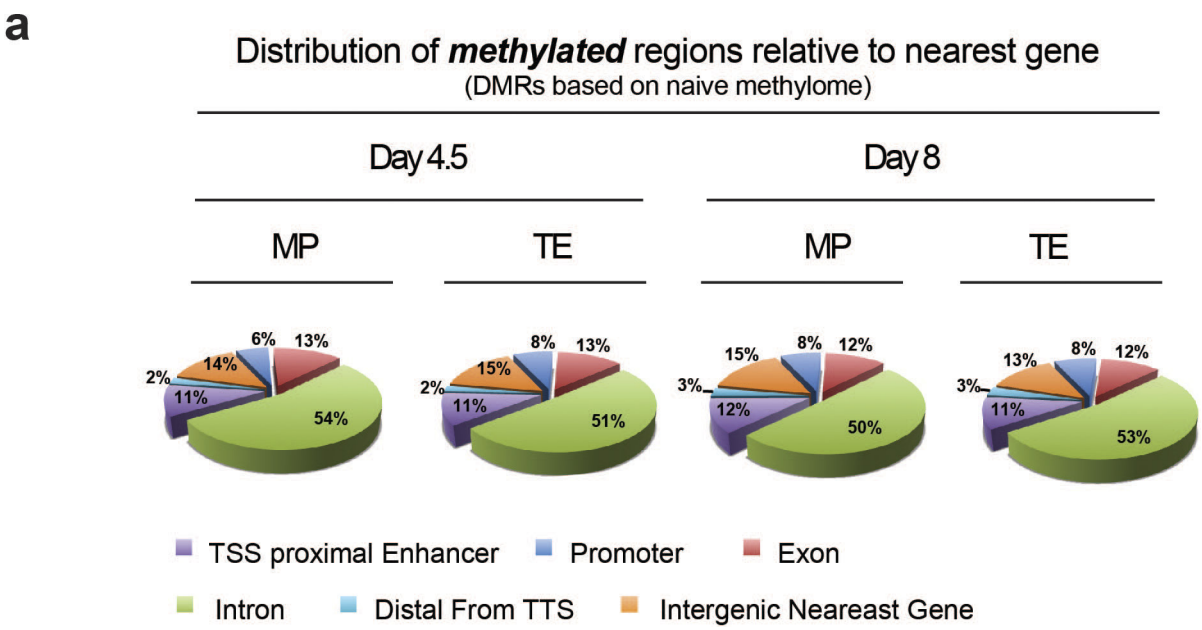

Extended Data Figure 3 | Effector-associated changes in DNA methylation occur predominantly at or near genes and are highly similar between MP and TE CD8 T cells. Pie chart representation of newly methylated DMR genomic distribution relative to the TSS of the nearest gene.

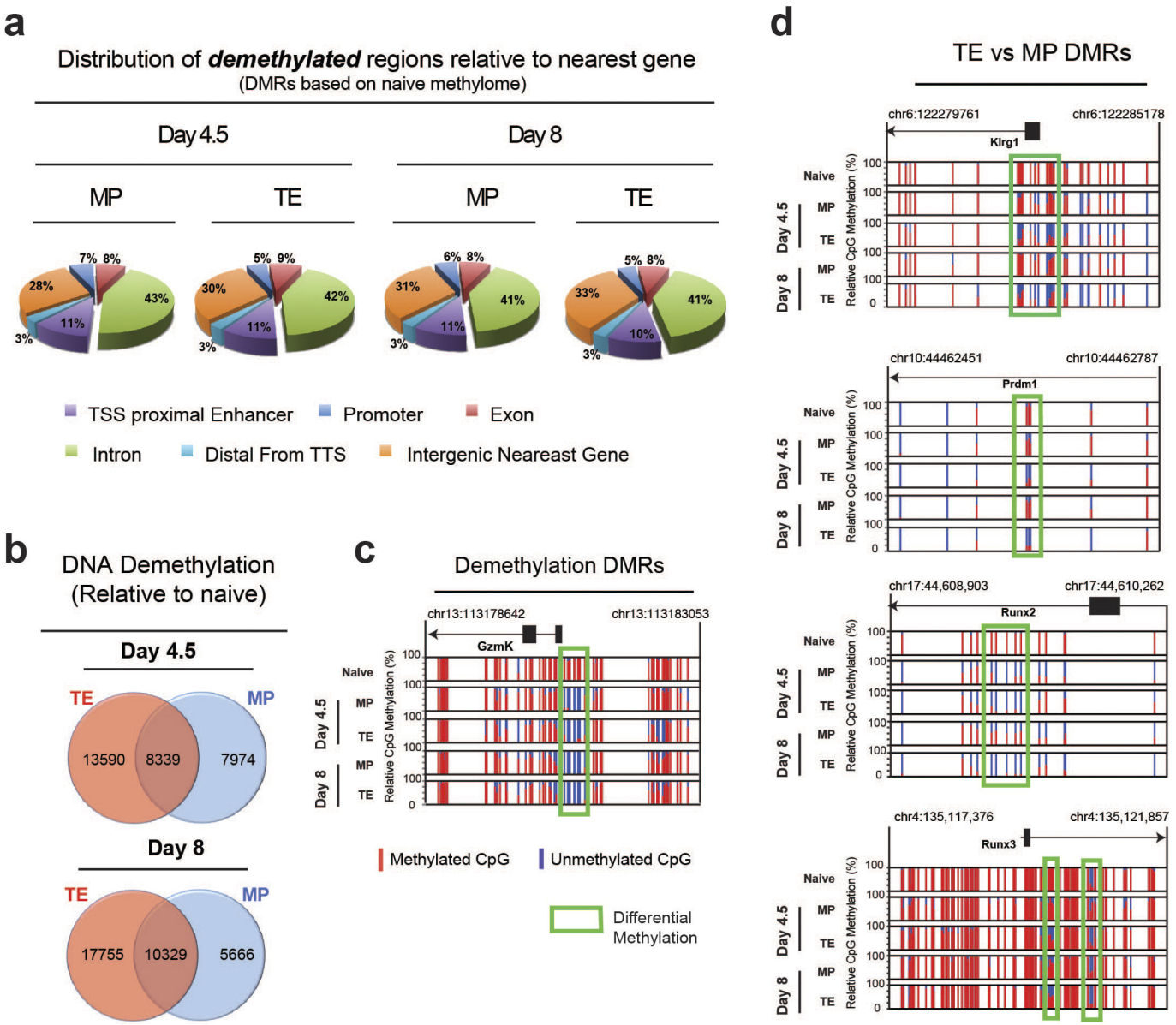

Extended Data Figure 4 | Both MP and TE CD8 T cells acquire demethylated effector loci. a, Pie charts represent demethylated DMR genomic distribution relative to the TSS of the nearest gene. **b**, Venn diagrams of regions that undergo demethylation during differentiation of naive CD8 T cells into TE and MP subsets. **c**, Normalized methylation at CpG sites in the *Gzmk* locus from TE and MP WGBS datasets. **d**, Normalized differentially methylated CpG sites in the *Klrg1*, *Prdm1* (also known as *Blimp1*), *Runx2*, and *Runx3* loci from TE and MP WGBS datasets.

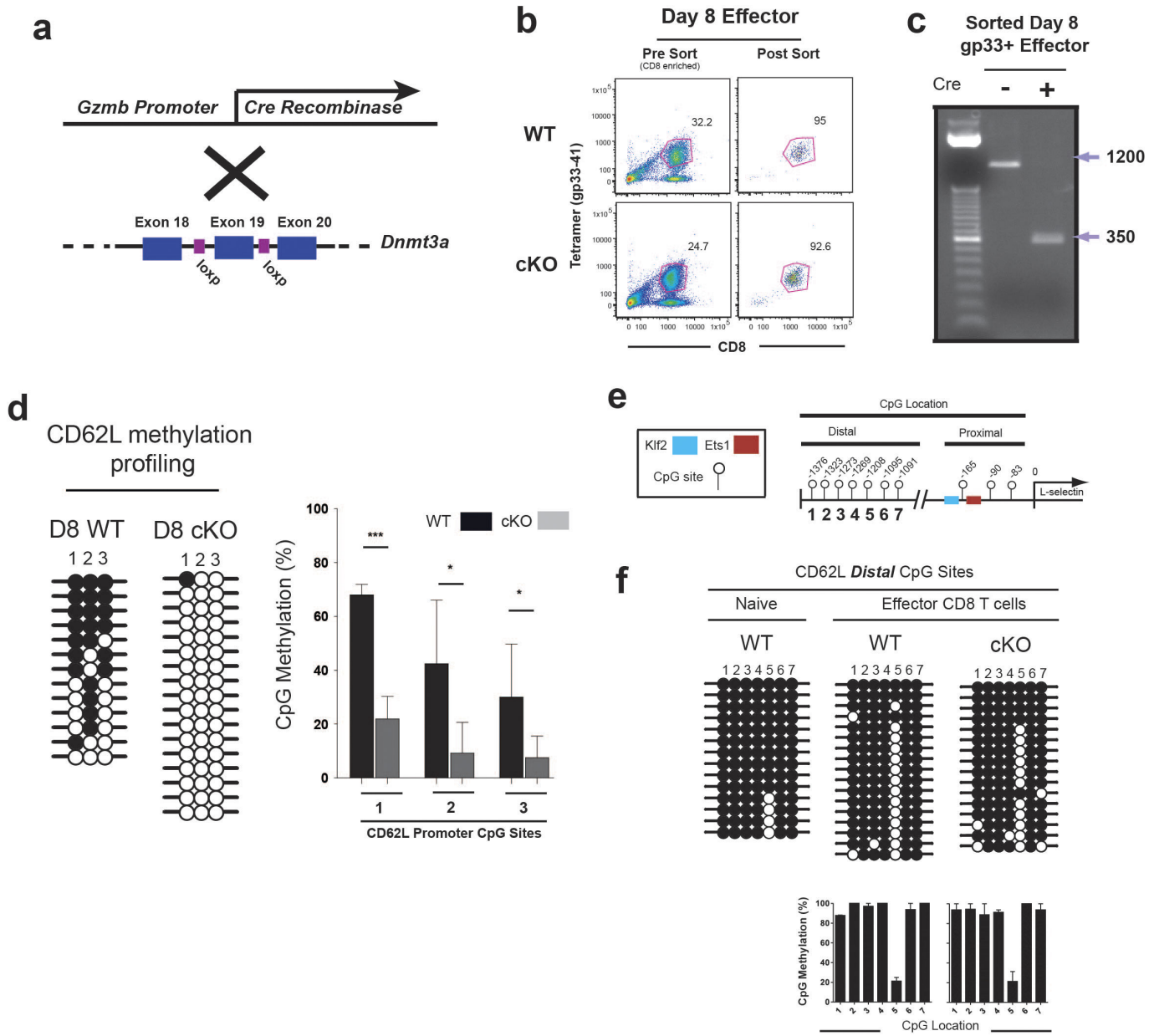

Extended Data Figure 5 | Conditional deletion of Dnmt3a in activated CD8 T cells inhibits effector-associated *de novo* DNA methylation but does not impair maintenance methylation. a, Cre recombinase expression is driven by the *Gzmb* promoter to initiate recombination of *Dnmt3a* exon 19 following T cell activation. **b**, Representative FACS analysis of virus-specific CD8 T cells sorted 8 days after acute viral infection of wild-type and *Dnmt3a* cKO mice. **c**, Recombination of genomic DNA from FACS-purified *Dnmt3a* cKO virus-specific CD8 T cells was assessed by PCR using primers that anneal to DNA outside the floxed target region. The larger PCR amplicon corresponds to the intact locus and the smaller PCR product is the amplicon of the recombined locus. **d**, Representative and graphical summary of *Sell* promoter methylation in wild-type and *Dnmt3a* cKO cells. Mean and s.d. were calculated from bisulfite sequencing analysis of six individually sorted populations. **e**, Diagram of *Sell* promoter CpG location proximal and distal to the TSS. **f**, Representative DNA methylation analysis of CpG sites distal to the *Sell* promoter regions in day 8 wild-type and *Dnmt3a* cKO antigen-specific effector CD8 T cells. Graphical summary of the average *Sell* distal CpG methylation in wild-type and *Dnmt3a* cKO cells calculated from bisulfite sequencing analysis of four individually sorted populations.

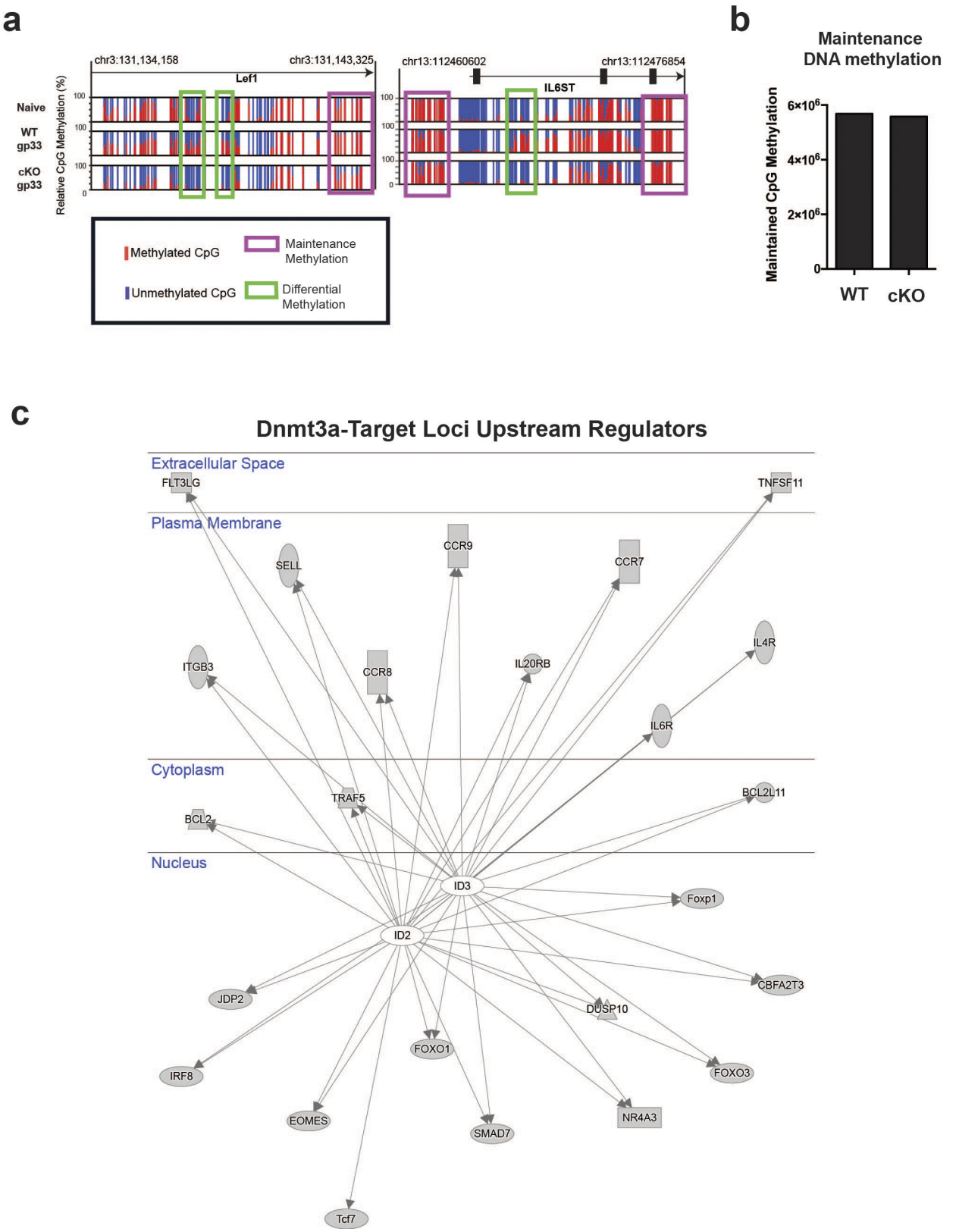

Extended Data Figure 6 | Effector-stage *de novo* DNA methylation is enriched at genes that regulate effector and memory T cell differentiation. a, Normalized Dnmt3a-mediated *de novo* methylation at CpG sites in the *Lef1* and *Il6st* loci from WGBS datasets. **b**, Summary of maintenance methylated regions in wild-type and *Dnmt3a* cKO effector WGBS datasets. **c**, Connectivity plot showing IPA-predicted interactions of ID2 and ID3 with Dnmt3a-targeted loci.

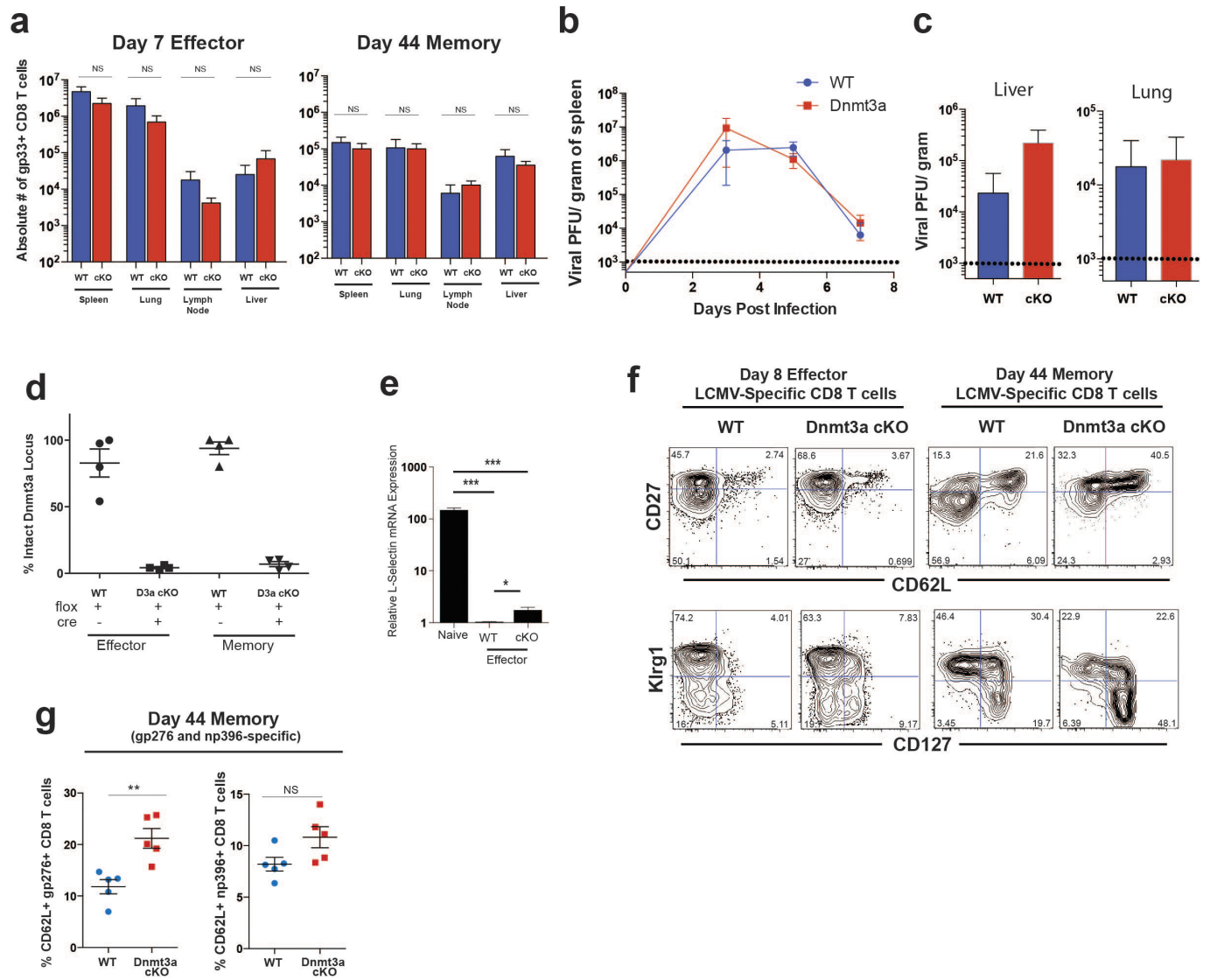

Extended Data Figure 7 | *Dnmt3a*-deficient CD8 T cells undergo effector differentiation. a, Summary of gp33-specific CD8 T cell quantities at effector and memory time points in lymphoid and nonlymphoid tissues. **b**, **c**, Summaries of viral titres in spleen (**b**) and day 5 lung and liver (**c**) of acutely infected wild-type and *Dnmt3a* cKO mice. **d**, Quantitative PCR analysis of *Dnmt3a* exon 19 recombination using a primer set that binds to DNA internal to the floxed target region. The mean and s.d. of intact (non-recombined) floxed *Dnmt3a* alleles were determined by quantitative PCR from four individually sorted gp33-specific effector and memory CD8 T cell populations. **e**, Real-time PCR analysis of *Sell* mRNA expression of naive and tetramer$^+$ wild-type and *Dnmt3a* cKO effector CD8 T cells. **f**, Representative FACS analysis of Klrg1, CD127, CD27, and L-selectin expression on wild-type and *Dnmt3a* cKO effector and memory gp33-specific CD8 T cell splenocytes. **g**, Summary graph for the percentage of wild-type and *Dnmt3a* cKO L-selectin-positive gp276 and np396-specific CD8 T cells.

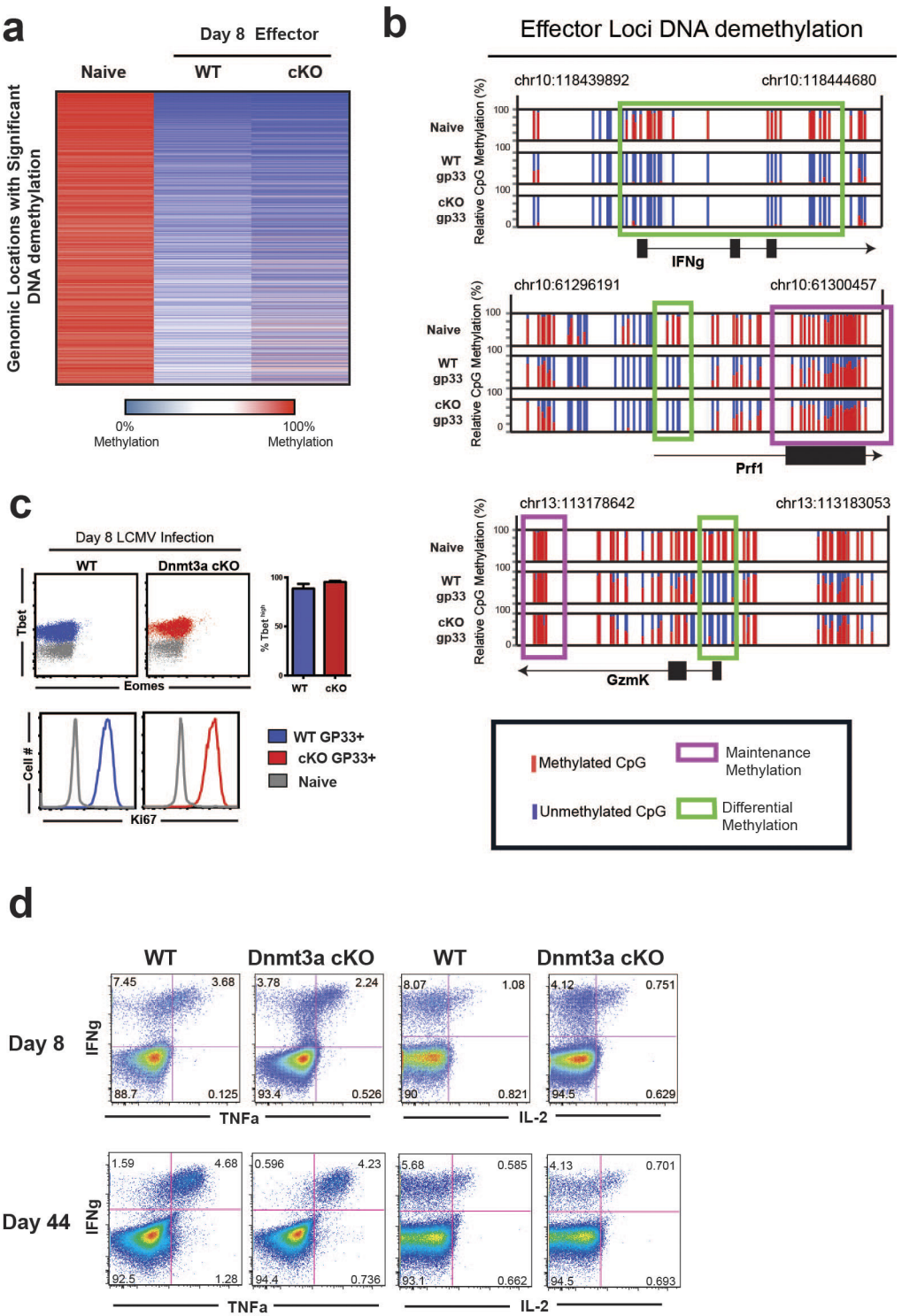

Extended Data Figure 8 | Effector molecule loci are demethylated during differentiation of virus-specific *Dnmt3a* cKO CD8 T cells. **a**, Heat-map representation of top 3,000 demethylated regions in wild-type and *Dnmt3a* cKO effector CD8 T cell WGBS datasets relative to the naive WGBS dataset. **b**, Normalized effector loci methylation at CpG sites in the *Ifng*, *Prf1*, and *Gzmk* loci from wild-type and *Dnmt3a* cKO WGBS datasets. **c**, Representative FACS analysis of Tbet, Eomes, and Ki67 expression of gp33-specific effector CD8 T cells. **d**, Representative FACS analysis of cytokine production from virus-specific memory CD8 T cells following 5 h of *ex vivo* gp33 peptide stimulation.

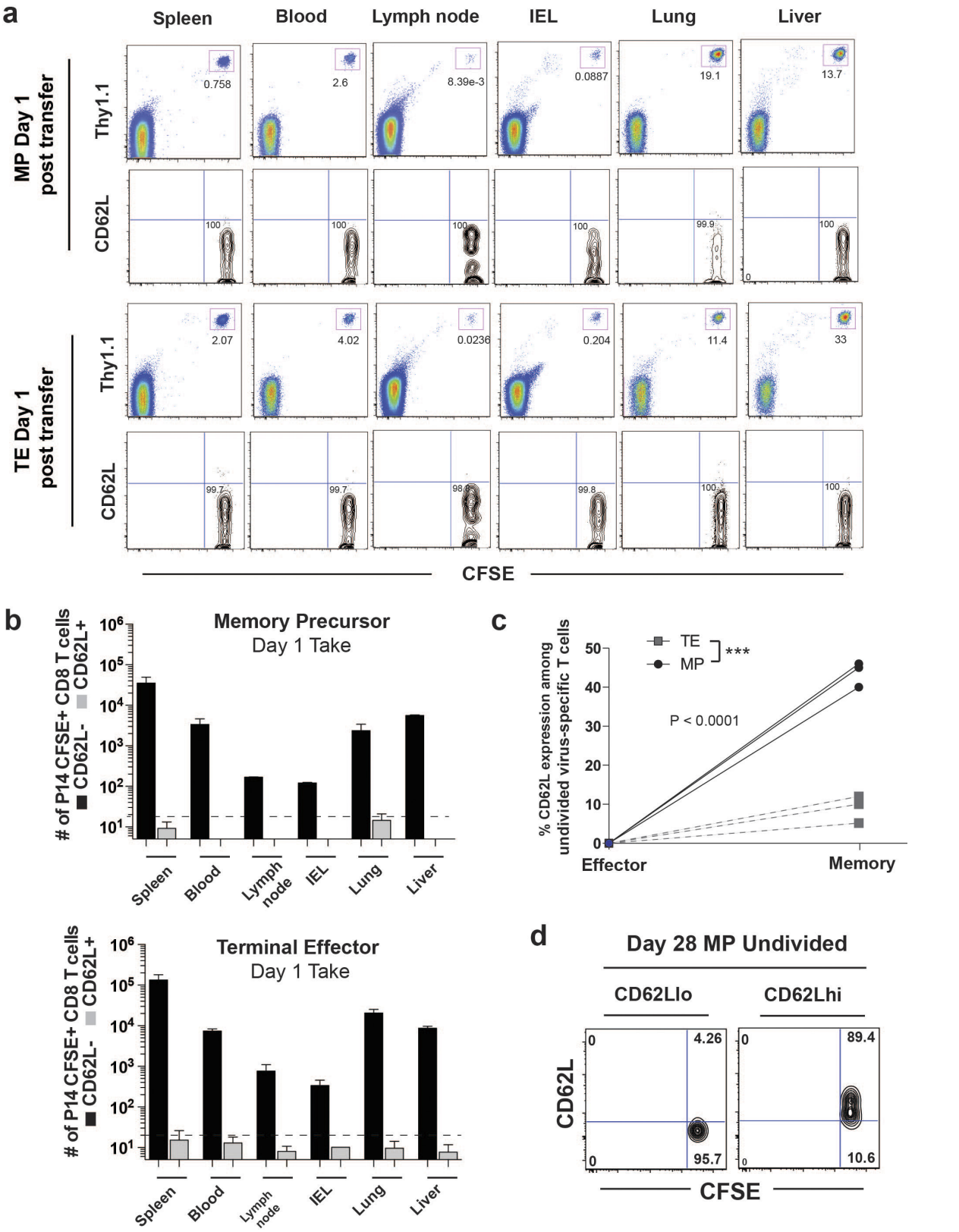

Extended Data Figure 9 | L-selectin^{lo} MP effector CD8 T cells develop into Tcm CD8 T cells. a, Representative FACS analysis of L-selectin expression on Thy1.1^{+} CFSE^{+} MP and TE CD8 T cells 1 day after transfer into naive recipient mice. The limit of our detection was approximately 10–20 CD62L^{+} cells in each of the lymphoid and nonlymphoid tissues at 1 day post-transfer. **b**, Summary of number of transferred TE and MP CD8 T cells in the spleen, blood, lymph node, IEL (intraepithelial lymphocytes), lung, and liver of the recipient mice 1 day post-transfer. **c**, Summary of per cent undivided (undiluted CFSE) L-selectin-positive virus-specific memory CD8 T cells arising from adoptively transferred MP versus TE cells. Data are from three independent experiments. **d**, Representative post-sort purity FACS analysis of undivided L-selectin^{hi} and L-selectin^{lo} MP P14 cells 28 days after adoptive transfer.

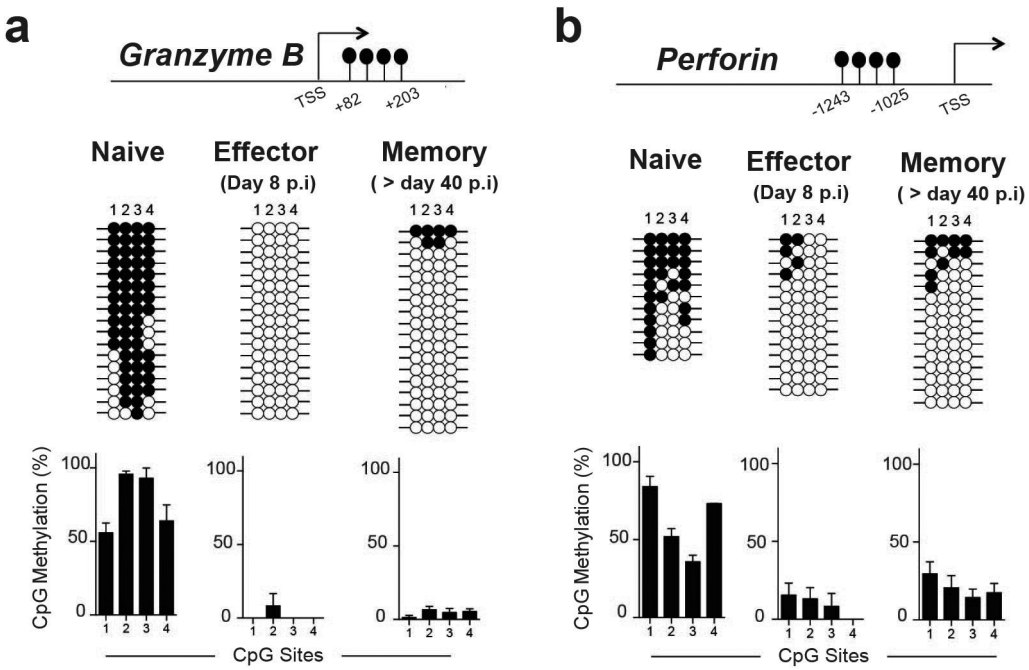

Extended Data Figure 10 | Memory CD8 T cells retain demethylated effector loci. Representative analysis and summary graphs of locus-specific methylation profiling of *Gzmb* (**a**) and *Prf1* (**b**) DMRs in naive, effector (day 8 gp33 tetramer$^+$) and memory (day 40+ gp33 tetramer$^+$) CD8 T cells. s.d. calculated from three independently sorted samples.

nature research

Corresponding author(s): Rafi Ahmed & Ben Youngblood

☐ Initial submission ☐ Revised version ☒ Final submission

Life Sciences Reporting Summary

Nature Research wishes to improve the reproducibility of the work that we publish. This form is intended for publication with all accepted life science papers and provides structure for consistency and transparency in reporting. Every life science submission will use this form; some list items might not apply to an individual manuscript, but all fields must be completed for clarity.

For further information on the points included in this form, see Reporting Life Sciences Research. For further information on Nature Research policies, including our data availability policy, see Authors & Referees and the Editorial Policy Checklist.

Experimental design

1. Sample size

Describe how sample size was determined.

The number of animals for each experiment were determined based on past experience with the model system. Bisulfite sequencing depth was determined using R as well based on previous experience.

2. Data exclusions

Describe any data exclusions.

Healthy male and female mice aged between 6-8 weeks were included in all studies without any additional exclusion criteria.

3. Replication

Describe whether the experimental findings were reliably reproduced.

All replication was successful

4. Randomization

Describe how samples/organisms/participants were allocated into experimental groups.

WT and conditional knockout mice were used as they became available from our breeding colony. Selection of mice was based on genotype without a plan for randomization.

5. Blinding

Describe whether the investigators were blinded to group allocation during data collection and/or analysis.

These studies were not blinded.

Note: all studies involving animals and/or human research participants must disclose whether blinding and randomization were used.

6. Statistical parameters

For all figures and tables that use statistical methods, confirm that the following items are present in relevant figure legends (or in the Methods section if additional space is needed).

n/a	Confirmed
☐	☒ The exact sample size (*n*) for each experimental group/condition, given as a discrete number and unit of measurement (animals, litters, cultures, etc.)
☐	☒ A description of how samples were collected, noting whether measurements were taken from distinct samples or whether the same sample was measured repeatedly
☐	☒ A statement indicating how many times each experiment was replicated
☐	☒ The statistical test(s) used and whether they are one- or two-sided (note: only common tests should be described solely by name; more complex techniques should be described in the Methods section)
☒	☐ A description of any assumptions or corrections, such as an adjustment for multiple comparisons
☐	☒ The test results (e.g. *P* values) given as exact values whenever possible and with confidence intervals noted
☐	☒ A clear description of statistics including central tendency (e.g. median, mean) and variation (e.g. standard deviation, interquartile range)
☐	☒ Clearly defined error bars

See the web collection on statistics for biologists for further resources and guidance.

Software

Policy information about availability of computer code

7. Software

Describe the software used to analyze the data in this study.	Prism for graphs. Flowjo for FACS plots.

For manuscripts utilizing custom algorithms or software that are central to the paper but not yet described in the published literature, software must be made available to editors and reviewers upon request. We strongly encourage code deposition in a community repository (e.g. GitHub). *Nature Methods* guidance for providing algorithms and software for publication provides further information on this topic.

Materials and reagents

Policy information about availability of materials

8. Materials availability

Indicate whether there are restrictions on availability of unique materials or if these materials are only available for distribution by a for-profit company.	No restrictions.

9. Antibodies

Describe the antibodies used and how they were validated for use in the system under study (i.e. assay and species).	Previously authenticated antibodies were purchased from BD, Biolegend, and Ebioscience. Citation of their use is below J ExpMed 2008; 205:625–640 PNAS. 2010 107(33):14733-8.

10. Eukaryotic cell lines

a. State the source of each eukaryotic cell line used.	ATCC
b. Describe the method of cell line authentication used.	Directly purchased from ATCC.
c. Report whether the cell lines were tested for mycoplasma contamination.	Not tested
d. If any of the cell lines used are listed in the database of commonly misidentified cell lines maintained by ICLAC, provide a scientific rationale for their use.	No commonly misidentified lines were used.

Animals and human research participants

Policy information about studies involving animals; when reporting animal research, follow the ARRIVE guidelines

11. Description of research animals

Provide details on animals and/or animal-derived materials used in the study.	Mouse, C57BL6, male and female, between 6 and 8 weeks of age.

Policy information about studies involving human research participants

12. Description of human research participants

Describe the covariate-relevant population characteristics of the human research participants.	This study did not involve human research

nature research

Corresponding author(s): Rafi Ahmed & Ben Youngblood

☐ Initial submission ☐ Revised version ☒ Final submission

Flow Cytometry Reporting Summary

Form fields will expand as needed. Please do not leave fields blank.

Data presentation

For all flow cytometry data, confirm that:

☒ 1. The axis labels state the marker and fluorochrome used (e.g. CD4-FITC).

☒ 2. The axis scales are clearly visible. Include numbers along axes only for bottom left plot of group (a 'group' is an analysis of identical markers).

☒ 3. All plots are contour plots with outliers or pseudocolor plots.

☒ 4. A numerical value for number of cells or percentage (with statistics) is provided.

Methodological details

5. Describe the sample preparation.	Cells were obtained from LCMV infected animals. Single cell suspension were obtained from PBMC or tissue as reported in the methods section
6. Identify the instrument used for data collection.	FACS canto
7. Describe the software used to collect and analyze the flow cytometry data.	Flowjo
8. Describe the abundance of the relevant cell populations within post-sort fractions.	FACS purities for sorted samples were >95%.
9. Describe the gating strategy used.	FSC/SSC to live to CD8 then the various markers as described in the figures and methods.

Tick this box to confirm that a figure exemplifying the gating strategy is provided in the Supplementary Information. ☐